Mobility of lower MA-helices for ion-conduction through lateral portals in 5-HT_{3A} receptors

Antonia G. Stuebler[1], Michaela Jansen[1]

[1]Department of Cell Physiology and Molecular Biophysics and Center for Membrane Protein Research, School of Medicine, Texas Tech University Health Sciences Center, Lubbock 79430, Texas, USA.

*Corresponding author: Michaela Jansen, Ph.D., Department of Cell Physiology and Molecular Biophysics, Center for Membrane Protein Research, School of Medicine, Texas Tech University Health Sciences Center, 3601 4th St., Lubbock, TX 79430. Tel: +1 806-743-4059; Fax: +1 806-743-1512; Email: michaela.jansen@ttuhsc.edu

Running Title: Mobility of MA-helices

Keywords: pentameric ligand-gated ion channels, serotonin, intracellular domain
(select 3 phrases and 3 techniques from a pre-determined list)

Statement of Significance: (120 words max)

The intracellular domain (ICD) of pentameric ligand-gated ion channels (pLGICs) is the most diverse domain within receptors of the Cys-loop superfamily. Despite being the least understood domain of pLGICs, we know that it influences channel function in multiple ways and shapes the cytosolic exit pathway of the channel. X-ray and cryo-EM structures have captured the structured segments of the ICD of 5-HT_{3A} receptors in different conformational states with lower resolution of the ICD as compared to the other domains. Here, we provide experimentally-derived evidence for the importance of the mobility of the MA-helices and functionally confirm ion-conduction through lateral portals as opposed to a vertical pathway for 5-HT_{3A} receptors.

Abstract:

Serotonin type 3A receptors (5-HT_{3A}Rs) are pentameric ligand-gated ion channels, pharmacologically targeted for the treatment of severe nausea and vomiting. The intracellular domain of 5-HT_{3A}Rs has been shown to be a crucial determinant for limiting conductance. Structurally, it consists of a short L1-loop following the third transmembrane segment M3, a short α-helical MX-segment, a large unstructured L2-loop, and the membrane-associated MA-helix that continues into the last transmembrane segment M4. During gating, conformational changes occur in all three domains. Extracellular and transmembrane domains rotate counterclockwise and clockwise, respectively. Within the intracellular domain the MA-M4 helix breaks at Gly430, leading to pore widening above and below the helix break, and the MX-helix moves outward and upward towards the membrane. At their bottom, the MA-helices come into close apposition to shape a narrow hydrophobic constriction below the cytosolic channel chalice that, in its upper section, is framed by lateral windows through which the L1-loops thread. In the present study, we used disulfide bond formation between pairs of engineered cysteines to probe the proximity and mobility of the bottom segments of the MA-helices. Repeated agonist application or oxidation induced a current run down for channels with Cys pairs at I409C/R410C. For Cys pairs at L402C/L403C these conditions did not lead to altered currents. On the contrary, cross-linked subunits for both L402C/L403C and I409C/R410C were observed for both conditions using gel electrophoresis. Our results indicate that the proximity and orientation for Cys in both pairs is conducive for disulfide bond formation. While conformational changes associated with gating promote cross-linking for I409C/R410C that in turn inhibits gating, cross-linking of L402C/L403C is functionally

silent. We infer that conformational changes associated with gating are more pronounced for the upper I409C/R410C pair in close proximity to the lateral windows as compared to the L402C/L403C pair at the apex of the inverted pentagonal pyramid contributed by the MA-helices.

Introduction

5-hydroxytryptamine 3 receptors (5-HT_3Rs) are pentameric ligand-gated ion channels (pLGICs) in the family of Cys-loop receptors, which also include the cationic nicotinic acetylcholine (nAChR), the anionic γ-amino butyric acid ($GABA_A$), and glycine receptors. Together these receptors are responsible for fast synaptic neurotransmission in the peripheral and central nervous system (Thompson and Lummis 2013). 5-HT_3 subunits assemble into the only ionotropic serotonin receptors. All other 5-HT proteins are G-protein coupled receptors (Thompson and Lummis 2007). The overall structure of pLGICs is conserved. Each subunit consists of three separate domains: the extracellular (ECD), transmembrane (TMD, M1-M4), and intracellular domains (ICD). The ICD of eukaryotic pLGICs between transmembrane segments M3 and M4 is the most diverse domain with regard to length (50-280 amino acids) and amino-acid composition across the family (Baptista-Hon, Deeb et al. 2013). 5-HT_{3A} receptor structures in multiple functional conformations have been obtained by X-ray crystallography and single-particle cryo-electronmicroscopy (cryo-EM) (Hassaine, Deluz et al. 2014, Basak, Gicheru et al. 2018, Basak, Gicheru et al. 2018, Polovinkin, Hassaine et al. 2018). Successively, these structures have also resolved segments of the ICD, which constitutes about one third of 5-HT_{3A} channels. More recently, structural studies of 5-HT_{3A} (Hassaine, Deluz et al. 2014, Basak, Gicheru et al. 2018, Basak, Gicheru et al. 2018, Polovinkin, Hassaine et al. 2018)

and nACh (Unwin 2005, Morales-Perez, Noviello et al. 2016, Walsh, Roh et al. 2018, Gharpure, Teng et al. 2019) discovered that the ICD consists of the following structural elements: a short post-M3 loop (L1), an amphipathic MX-helix, a long loop (L2) of 60 unresolved amino acids, and the membrane-associated helix (MA-helix). The MA-helix of 31 amino acids (Miyazawa, Fujiyoshi et al. 1999)) is continuous with the M4-transmembrane segment. The ICD is crucial for the functionality of the entire receptor: it contributes to desensitization and gating mechanisms, single-channel conductance, receptor sorting and trafficking by interacting with intracellular proteins, as well as inward rectification and Ca^{2+} permeability (Halevi, McKay et al. 2002, Halevi, Yassin et al. 2003, Kelley, Dunlop et al. 2003, Jansen, Bali et al. 2008, Livesey, Cooper et al. 2008, Goyal, Salahudeen et al. 2011, Papke and Grosman 2014, Mnatsakanyan, Nishtala et al. 2015, Pirayesh, Stuebler et al. 2019). The ICD is known to limit the single-channel conductance to sub-pS levels for the 5-HT_{3A} homomer (Kelley, Dunlop et al. 2003). The portals for ion access at the cytosolic side of the transmembrane ion channel have been inferred to be framed by the MA-helices of the ICD based on the observation that a triple amino acid substitution construct, namely RRR to QDA (R432Q/R436D/R440A), increased the single-channel conductance ~33-fold (Kelley, Dunlop et al. 2003, Carland, Cooper et al. 2013). Two possible exit pathways for ions were seen in the X-ray structure (Hassaine, Deluz et al. 2014): one through the five lateral portals, and another through a vertical portal in continuation with the pore of the transmembrane channel. The pore diameter of the vertical pore in the crystal structure is larger in even non-conducting states (4.2 Å) but has a 17-Å-long narrow zone lined with hydrophobic residues on the inside of the pore (Hassaine, Deluz et al. 2014). More recently, density for a lipid was observed in this

segment in a full-length nAChα4β3 cryo-EM structure resulting in a 'hydrophobic plug' (Gharpure, Teng et al. 2019). The lateral portals, on the other hand, are obstructed by the L1-loop threading through them (Hassaine, Deluz et al. 2014, Basak, Gicheru et al. 2018). Newer cryo-EM structures captured the 5-HT_{3A}R in its presumably open state with the lateral portals in a conformation conducive for ion translocation, a difficult task considering its fast rate of desensitization (Basak, Gicheru et al. 2018, Polovinkin, Hassaine et al. 2018).

The overall movement of the receptor entails a global twisting of the ECD and TMD around the central pore (counterclockwise and clockwise for ECD and TMD, respectively), similar to other pLGICs (Sauguet, Shahsavar et al. 2014, Du, Lu et al. 2015). Some earlier noteworthy studies have shown that the binding of the agonist transmits a conformational change to the ICD, measured by fluorescence with the enhanced green fluorescent protein (EGFP) located in L2 in close proximity to the MA-helix (Ilegems, Pick et al. 2005). When comparing the conducting with the non-conducting structures of the 5-HT_{3A}R (Fig. S1), differences in the conformation of the ICD, in particular surrounding the vertical portals, can be observed: in the conductive conformation the MA-M4 helix breaks at Gly430 and tilts away from the pore axis to open up the TMD-ICD interface cavity and the MX-helix moves outward and upward towards the membrane. This MX-helix motion pulls the L1-loop through the portals. Overall, these concerted motions yield a conductive conformation for the lateral portals (Basak, Gicheru et al. 2018).

In this study, we investigated the mobility of the lower end of the MA-helices. We engineered Cysteine pairs, three and five helical turns below the lateral portals, and used disulfide trapping to probe the movement at two different levels of the ICD. Through our

experiments, we demonstrate that mobility of the MA-helices just below the lateral portals is required to open the cytosolic ion access pathway. On the contrary inhibiting mobility at the very bottom of the MA-helices had no functional effect on ion-conduction through the lateral portals.

Materials and Methods

Materials

Copper(II) sulfate pentahydrate (Sigma-Aldrich, St. Louis, MO); 1,10-Phenanthroline (Sigma-Aldrich, St. Louis, MO); NEM (*N*-Ethylmaleimide, Sigma-Aldrich, St. Louis, MO); DTT (dithiothreitol, Fisher Scientific, Fair Lawn, NJ); EGTA (Ethyleneglycol- bis(β-aminoethyl)-N,N,N',N'-tetraacetic acid tetrasodium ≥97%, Sigma-Aldrich, St. Louis, MO); 5-HT (serotonin hydrochloride Sigma-Aldrich, St. Louis, MO). Stock of serotonin (2 mM), copper(II) sulfate (100 mM), and DTT (1 M) were prepared in distilled water. 1,10-Phenanthroline (0.5 M) was dissolved in dimethyl sulfoxide (DMSO). All solutions, including the Cu:Phe solution, were made in oocyte ringer buffer (OR-2) immediately before experiments were conducted.

Molecular Biology

Cysteine were engineered into mouse 5-HT_{3A}R (AAT37716), containing a V5-tag (GKPIPNPLLGLDSTQ) close to the N-terminus (Jansen, Bali et al. 2008), in the pGEMHE vector for oocyte expression (Reeves, Goren et al. 2001). The desired base pairs coding for Cys were introduced using overlapping primers with the QuikChange II SiteDirected Mutagenesis kit (Agilent Technologies) and were confirmed by DNA sequencing

(GENEWIZ, South Plainfield, NJ). The numbering used corresponds to the numbering of the mature sequence as published with the X-ray structure (Hassaine, Deluz et al. 2014). There are three intrinsic cysteines in the ICD of 5-HT_{3A}, two in the L2-loop and one ~40 Å apart from the engineered cysteine residues (Hassaine, Deluz et al. 2014). cDNA was linearized with the *Nhe*I restriction enzyme and subsequently in vitro transcribed with the T7 RNA polymerase kit (mMESSAGE mMACHINE® T7 Kit; Applied Biosystems/Ambion, Austin, TX). cRNA was purified with the MEGAclear™ Kit (Applied Biosystems/Ambion, Austin, TX), and precipitated using 5 M ammonium acetate. The cRNA was subsequently dissolved in nuclease-free water and stored at -80 °C.

Xenopus laevis **oocyte preparation and injection**

Xenopus laevis (*X. laevis*) oocytes were isolated, enzymatically defolliculated, and stored as previously described (Stuebler and Jansen 2019). *X. laevis* were handled and maintained following procedures approved by the local animal welfare committee (Institutional Animal Care and Use Committee, IACUC #: 08014, PHS Assurance # A 3056-01). Before injection, oocytes were washed in oocyte ringer's solution (OR-2: 115 mM NaCl, 2.5 mM KCl, 1.8 mM MgCl2, 10 mM HEPES, pH 7.5) and maintained in standard oocyte saline medium (SOS: 100 mM NaCl, 2 mM KCl, 1 mM $MgCl_2$, 1.8 mM $CaCl_2$, 5 mM HEPES, pH 7.5, supplemented with 1% Antibiotic-Antimycotic (100X, 10,000 units/mL of penicillin, 10,000 mg/mL of streptomycin and 25 mg/mL amphotericin B, Gibco, Thermo Fisher Scientific), 5% horse serum) for up to 7 days at 16 °C. Oocytes were microinjected with 10 ng of *in vitro* synthesized cRNA (200 ng/µL) using an automatic oocyte injector (Nanoject II™; Drummond Scientific Co., Broomall, PA).

Depending on the construct injected, sufficient expression could be seen 24-48 hrs after injection.

Electrophysiology

Two-electrode voltage clamp recordings were conducted 1-3 days after injection. The current were recorded and amplified using a TEV-200A amplifier (Dagan Instruments, Minneapolis, MN), a Digidata 1440A data interface (Molecular Devices, Sunnyvale, CA), and MiniDigi 1B (Molecular Devices), all controlled by pClamp 10.7 software (Molecular Devices). The oocytes were perfused with OR-2 using gravity flow at an approximate rate of 5 mL/min in a 250 µL chamber. The reagents (Cu:Phe, DTT, and EGTA) were dissolved in OR-2 and perfused in the same manner. All experiments were performed at room temperature (RT, 22–24°C) and a holding potential of -60 mV. The glass pipettes were filled with 3 M KCl and had a resistance below 2 MΩ. Current were evoked by 3 µM 5-HT, unless otherwise stated, and the agonist was applied until a stable response was observed to record maximal current response.

Oocyte Protein Isolation

X. laevis oocytes expressing 5-HT_{3A}Rs and constructs were incubated in 100:200 µM Cu:Phe for 2 min before being homogenized. A crude membrane protein fraction was isolated as described before (Pandhare, Pappu et al. 2017). In brief, the oocytes were homogenized using a 200 µL pipette tip in ice-cold vesicle dialysis buffer (VDB: 100 uL/oocyte: 96 mM NaCl, 0.1 mM EDTA, 10 mM MOPS, 0.02% NaN_3, 2 mM NEM , pH 7.5), supplemented with protease inhibitor cocktail III (PI, 2 µL/mL; Research Products

International, Mt. Prospect, IL) and centrifuged (800 g for 10 min at 4 °C). The supernatant was collected and proteins were obtained by high-speed centrifugation (39,000 g for 1 h at 4 °C). The crude membrane pellet was resuspended in VDB without NEM (3 µL/ oocyte) containing PI cocktail and stored at -80 °C.

Western Blotting

For SDS-electrophoresis, total protein fractions, as well as uninjected oocytes as control, were separated using 4–15% precast gradient TGX Stain-Free$_{TM}$ gels (Bio-Rad Laboratories) for 35 min at 200 V. Proteins were transferred to PVDF membranes using the Trans-Blot Turbo Transfer System (Bio-Rad). Membranes were blocked with 5% blotting-grade blocker (Bio-Rad) in Tween-tris-buffered saline (TTBS, 100 mM Tris, pH 7.5, 0.9% NaCl, 1% Tween-20) [25 – 30 mL/membrane]) overnight. The membranes were incubated with the primary V5 HRP-conjugated antibody (1:5,000, V5-HRP antibody, Invitrogen) in TTBS with 5% blotting-grade blocker overnight at 4 °C. After the removal of the primary antibody, the membranes were washed 5 times for 5 min with TTBS. Proteins were visualized by chemiluminescent detection (ImageQuant LAS 4000, GE Healthcare Life Sciences) of peroxidase substrate activity (SuperSignal West Femto Maximum Sensitivity Substrate, Thermo Scientific).

Data Analysis

All data was analyzed using pClamp, Origin (OriginLab Corporation: Northampton, MA), Prism 6 Software (GraphPad Prism®; La Jolla, CA), and UN-SCAN-IT *gel*$_{TM}$ (Silk Scientific, Inc.: Orem, UT). Data is shown as mean ± S.D. (n≥3) with the maximal current

induced by 5-HT as the normalizing standard (100% of current response) for other current amplitudes recorded in the same oocytes. Statistical significance was determined with paired t-test between the initial inward current and each set of conditions or one-way ANOVA, Dunnett's multiple comparisons test (*$p \leq 0.05$ **$p \leq 0.01$ ***$p \leq 0.001$). All figures and graphs were made in Origin, PyMOL Molecular Graphics System (Schrödinger, LLC), and Adobe Illustrator CC 2018.

Results

In order to investigate the mobility of the lower part of the intracellular domain of 5-HT_{3A}R, we designed two different double-cysteine constructs (Fig 1). For each double-Cys construct, we engineered two individual, adjacent cysteines per subunit to enable, in theory, cross-linking of all five subunits within one receptor. Both double-Cys pairs were introduced below the proposed lateral portals at different levels in the ICD, almost two helical turns apart (Fig 1, yellow: L402C/L403C, magenta: I409C/R410C). The distances between the cysteines' α-carbons of adjacent subunits are ~6.1 Å and ~5.7 Å for L402C/L403C and I409C/R410C, respectively (Fig 1A (Hassaine, Deluz et al. 2014)). The average Cα-Cα' carbon distance is 5.6 Å between disulfide-bonded cysteines (Careaga and Falke 1992, Schmidt, Ho et al. 2006). Double-cysteine pairs were introduced in the 5-HT_{3A}- and high-conductance QDA-backgrounds, respectively.

We injected cRNA for all 5-HT_{3A}R constructs into *X. laevis* oocytes. Current amplitudes were measured in response to application of 3 μM 5-HT. This 5-HT concentration is ~5-fold above EC_{50} values for 5-HT_{3A}, QDA, and QDA-409/10 (Jansen, Bali et al. 2008). All constructs exhibited 5-HT-induced currents (Fig 2). The inward current responses of 5-

HT_{3A} and 5-HT_{3A}-QDA receptors (Fig 2, top panel) were stable (variations<10%), and introduction of the double-Cys pair L402C/L403C did not alter the stability of the current responses to 5-HT application (Fig 2, middle panel). On the other hand, 5-HT-evoked inward current amplitudes of the double-Cys pair I409C/R410C steadily declined with repeated agonist-application (Fig. 2, bottom panel) until a stable level was reached, ~38% and ~27% of the original current, for 3A-409/10 and QDA-409/10, respectively (Fig. 5). This stable level of significantly attenuated current amplitude could also be achieved by prolonged 5-HT exposures of 2 min and did not require a repeated application of 5-HT (Fig 3). A single Cys introduced at 409 alone lead to stable responses to agonist application (Fig. S2).

1,10-Phenanthroline in the presence of copper (Cu:Phe) is a catalyst for oxidation of sulfhydryl groups to disulfides. The Cu:Phe oxidative mechanism involves diffusible reactive intermediates that can penetrate protein interiors (Kobashi 1968, Amin, Taylor et al. 2006, Bass, Butler et al. 2007). We assessed the effect of this reagent on the double-Cys pairs by exposing oocytes expressing 5-HT_{3A}Rs constructs to a concentration of 100:200 μM Cu:Phe for 2 min (Fig. 4A, Fig. S3A) following the initial inward current response evoked by 5-HT (Jansen and Akabas 2006, Wiltfong and Jansen 2009, Mnatsakanyan and Jansen 2013). This first inward current was tested for stability in 5-HT_{3A}Rs and all constructs, except in 3A-409/10 and QDA-409/10 due to the current decrease observed with repeated agonist application (Fig. 2). After the 2 min application of Cu:Phe, the oocytes were washed for 6 min with OR-2 before another agonist-induced current was recorded (Fig 4A, second inward current) and tested for stability. Lastly, we investigated the effect of applying 10 mM DTT (Fig. 4A, Fig. S3A), a reducing agent

capable of converting protein disulfides to sulfhydryls via thiol-disulfide exchange reaction, or 1mM EGTA (Fig. 4B, Fig. S3B), a chelating agent capable of binding excess copper ions (Fisher, Hague et al. 2004). DTT or EGTA was applied to the same oocyte for 2 min, followed by a 6 min OR-2 wash before another 5-HT application (final inward current, DTT: Fig 4A, EGTA: Fig 4B).

Overall, 5-HT-induced inward currents of 5-HT_{3A} were unaffected by Cu:Phe and DTT but showed a ~15%-increase in amplitude after perfusion with EGTA (Fig. 4 and 5, Fig. S3). The current amplitudes of QDA and 3A-402/3 showed no change after Cu:Phe or EGTA, however increased by ~12% and ~14%, respectively, after exposure to DTT (Fig. S3, Fig. 5). The same Cys pair in the QDA-background, QDA-402/3, showed reduced current amplitudes after Cu:Phe (71.7±11.6% of initial, n=12) as compared to the initial current, which could be recovered by either DTT or EGTA. Overall, Cu:Phe had the most pronounced effect on 3A-409/10 and QDA-409/10, decreasing their inward current amplitudes to ~61% and ~29% of the initial inward current, respectively. An effect not observed in the single Cys construct (Fig. S2). In the case of 3A-409/10, the current response after Cu:Phe was not stable and the amplitude was further reduced to ~39% with repeated agonist application (Fig 4. Middle panel, third inward current evoked by 5-HT in sample traces, Fig 5). This reduction in current response could not be recovered for 3A-409/10 and could be partially recovered with DTT for QDA-409/10 (61.6±8.32% of initial current).

Proteins expressed in *X. laevis* oocytes were additionally visualized by Western blot after SDS-polyacrylamide gel electrophoresis (Fig. 6) under oxidizing and reducing conditions, as well as the presence of agonist (van Montfort, Schuurman-Wolters et al. 2001, Lee

and Gouaux 2011). The 5-HT_{3A}R and all of the constructs contain a V5-epitope tag near the N-terminus. *X. laevis* oocytes were exposed to 3 μM 5-HT or 100:200 μM Cu:Phe for 2 min before they were homogenized to generate total membrane protein fractions, each condition containing 16+ oocytes. The final pellet was resuspended in VDB and was run on SDS-PAGE either with or without DTT. Using Western blots, 5-HT_{3A} channels were detected via V5-epitope tag (Fig. 6A). The band intensities varied with different oocyte expression levels and were adjusted accordingly. The different band intensities were quantified (UN-SCAN-IT *gel*$_{TM}$) and are shown as percentages (Fig 6B, normalized to the monomer band set at 100%) for each oligomeric state and each construct. 5-HT_{3A}Rs and constructs have monomer bands at ~55 kD but only the double-Cys pairs show higher oligomeric states, with an increased amount in the QDA-background as compared to WT (Fig. 6B). The addition of DTT in the running dye with the crude membrane fractions of oocytes previously exposed to Cu:Phe abolished all oligomers (Fig. 6A, lowest panel).

Discussion

The ICD is the most diverse, yet least understood domain of pLGICs. The first structure of 5-HT_{3A} based on X-ray crystallography did “not offer an exit pathway for the ions” (Hassaine, Deluz et al. 2014) The ion-conduction pathway previously predicted for nAChRs (Miyazawa, Fujiyoshi et al. 1999) through five lateral cytosolic portals was obstructed by a post-M3 loop threading though the portals. As a consequence, the question was raised whether ions would exit through the lateral portals, requiring conformational changes of the post-M3 loop and MX-helix, or along the channel axis. Structural insights into the mechanism were recently provided by cryo-EM structures in

different functional states (Basak, Gicheru et al. 2018). The recent cryo-EM 5-HT_{3A} structures features a drastic conformational change in the MX-helix of the ICD to open five lateral portals for cations to exit to the cytosol (Fig. S1, (Basak, Gicheru et al. 2018)). The only other α-helical structure in the ICD, the MA-helix, has shown to affect channel function: influencing Ca^{2+}-permeability and single-channel conductance (Kelley, Dunlop et al. 2003, Livesey, Cooper et al. 2008). Most noteworthy, the MA-helices of 5-HT_{3A} are lined with positively and negatively charged residues that interact to form inter- and intra-subunit salt bridges, a characteristic specific to the A subunit (Kozuska, Paulsen et al. 2014, Pandhare, Pirayesh et al. 2019). The five lateral portals are located between adjacent MA-helices and amino acid substitutions introduced in their proximity leads to the breaking of these salt bridges, which enhances flexibility of the MA-bundle, increases single-channel conductance, and disrupts pentamerization of the ICD (Kelley, Dunlop et al. 2003, Kozuska, Paulsen et al. 2014, Pandhare, Pirayesh et al. 2019). Another notable salt bridge is located between the MA-helix and the L1-loop: D312 at the center of L1 is straddled by arginine residues (R436 and R440) from the MA-helix of the adjacent subunit.

In the present study, we investigated the extent of mobility of the cytosolic end of the MA-helices of 5-HT_{3A} by using disulfide bond formation between engineered cysteines. Disulfide trapping is a powerful tool to analyze backbone and domain motions in a protein of known high-resolution structure with the advantage that these experiments can be carried out in the native environment of the protein (Careaga and Falke 1992, Bass, Butler et al. 2007).

We engineered double-Cys pairs within the MA-helix of 5-HT_{3A} subunits with the goal of using intersubunit disulfide bonds between adjacent subunits to clamp the MA-helices in a tight narrow conformation that impedes ion flow and gain insight into their conformational/ rotational movement. The same Cys-pairs were introduced into the QDA-background that has a ~33-fold increased conductance. Based on our observation that the QDA substitution abolishes pentamerization of the ICD in the absence of the other two domains, we hypothesize that partial release of intersubunit salt-bridges in the QDA background yields a more open and unclamped/flexible arrangement of the ICD, in particular the MA-helices (Pandhare, Pirayesh et al. 2019). The Cys substitutions were introduced three and five helical turns below the last arginine (R420) located in the vertical portals, the part of the MA-helix that so far has been orphaned by functional studies.

The double-Cys pairs 3A-409/10 and QDA-409/10 interestingly showed spontaneous disulfide bond formation with agonist application, indicated by the decrease in current amplitude with repeated or extended applications of 5-HT until a steady state was reached (~40% and ~22% of the first inward current respectively, Fig 2, Fig 3, and 5). Disulfide bond formation of cysteine residues depends on the presence of an oxidizing environment as well as the sulfhydryl collision frequency, which is influenced by their separation distance, their orientation in the protein, and the backbones mobility in the region (Bera and Akabas 2005). Spontaneous cross-linking indicates a relatively high propensity for this disulfide bond formation, and fundamentally does not differ from cross-linking in more oxidizing environments created by Cu:Phe (Bera and Akabas 2005, Borghese, Hicks et al. 2014). A more oxidizing environment (100:200 μM Cu:Phe) also lead to disulfide bond formation (current reduction to 60.8±12.1% and 28.6±13.6% for 3A-

409/10 and QDA-409/10, respectively, Fig 4 and 5). For 3A-409/10, the current responses tested after oxidation were not stable and current amplitudes were further reduced by repeated applications of 5-HT to 39.2±15.4%, similar to the reduction obtained by agonist-induced cross-linking alone (Fig 4 second panel and Fig 5), suggesting that serotonin induces a motion in the receptor that promotes disulfide bond formation at these positions (Chrisman, Podair et al. 2014). This reduction in current amplitude could neither be recovered with reducing nor chelating agent. Based on the mechanism of the involved redox chemistry, reduction with DTT involves a disulfide exchange reaction, necessitating access of the DTT molecule in close apposition to the disulfide bond to be reduced. Therefore, the inability to reverse oxidation with DTT may be due to the reduced accessibility of the less mobile and rigid MA-bundles in the WT background (Kozuska, Paulsen et al. 2014). For QDA-409/10 on the other hand, cross-linking was partially reversed with DTT but not the chelating agent EGTA, indicating that the reduction in current is caused by disulfide bond formation and not heavy metal binding. Additionally, the partial reversibility in the QDA background compared to the irreversibility in the WT background further points towards increased mobility mediated by the QDA substitutions. The spontaneous disulfide bond formation of I409C/R410C with agonist application yields two subsets of information. Firstly, disulfide bonds have well-defined distance and angular constraints, which indicates close proximity for the two Cys when a Cystine forms (Careaga and Falke 1992). Secondly, disulfide bond formation at I409/R410 locks a large fraction of channels in a non-conducting state by putting structural constraints on the mechanism of conformational changes (de la Pena, Alonso-Ron et al. 2011), giving insights into the relationship between structural changes and function. We observed

spontaneous disulfide bond formation after the application of the agonist. In the presence of 5-HT, the channels undergo transitions between several different open, desensitized, and closed states. We cannot, with certainty, distinguish in which state spontaneous disulfide bond formation occurs due to the millisecond timescale of transitioning (Bera and Akabas 2005, Jansen and Akabas 2006). Based on structures of 5-HT_{3A} in different states and our data, the MA-helices are in closest proximity when the channel is desensitized or transitioning from an open to a closed conformation (Fig. S1, Table 1)(Chrisman, Podair et al. 2014).

For the other double-Cys pair, 3A-402/3 and QDA-402/3, minimal oxidizing reagent-induced current reduction (~96% and ~72% of initial current for 3A-402/3 and QDA-402/3) and reductant-induced reversal were observed (Fig. 5 and Fig. S3, orange and yellow). Both pairs show current recovery after DTT and also EGTA incubation (~115% and ~97% of control current for 3A-402/3 and QDA-402/3, Fig. 5). This could indicate an alleviation of a small inhibitory effect of heavy-metal binding (Fig. S3, Fig. 5). Although we could not observe a clear pattern of functional effects for this Cys pair, proteins visualized on western blot showed cross-linking between subunits manifested as bands representing monomers and oligomers for both double-cysteine constructs (Fig 6A)(Bali, Jansen et al. 2009). The higher oligomers were only observed for the cysteine pairs and not WT or QDA in the presence of agonist or oxidizing agent. The overall quantification of band intensities for each construct in each condition revealed that the Cys pairs in the QDA-background show higher percentages for dimers and some higher oligomeric states as compared to the WT-background (Fig. 6B). Consistent with our functional experiments, this effect could be due to the QDA-substitution breaking important salt-bridges, which

lead to an increase in flexibility of the MA-helices. These covalently-linked oligomers could be completely reduced to monomers in the presence of a reducing agent (Fig. 6A bottom panel). Our results indicate that cross-linking of L402C/L403C is functionally silent, which indicates their proximity to each other in the equilibrium structure (Bass, Butler et al. 2007) and in turn, supports the structural prediction for five lateral portals (Basak, Gicheru et al. 2018).

Overall, we conclude that disulfide bonds form for both double-cysteine pairs. We infer that conformational changes associated with gating are more pronounced for the upper I409C/R410C pair that sits three helical turns below the frame of the lateral windows and on the upper end of the hydrophobic plug. The area below this plug, where the helices converge, seems to be involved in smaller motions while the ICD above twists around the central pore of the receptor. These findings can be compared to the mechanics of an umbrella, where the MA-helices represent the rods of the umbrella. In the inverted umbrella the ferrule/top notch corresponds to the cytosolic end of the MA-helixes. Low on the converging rods/MA-helices we find L402C/L403C whereas I409C/R410C is positioned towards the top of the rods (Fig. 7). When the umbrella is closed (aka. the receptor is in a non-conducting state) the rods are aligned with the shaft (ion pore), in a vertical line, and both the lower (L402C/L403C) and upper portion (I409C/R410C) of the rods are in close proximity to corresponding adjacent rod positions. When the umbrella opens, the upper rod positions (I409C/R410C) move outward to allow for the canopy to open, while the lower positions closer to the notch (L402C/L403C) remain relatively stationary at the end of the shaft. Structures indicate a clockwise rotational movement of the TMD (Basak, Gicheru et al. 2018) between closed and open states. The TMD is

structurally linked to the ICD by the continuation of the M4 transmembrane segment into the MA-helix. The twisting movement of MA-helices breaks the salt bridge network, including D312, which holds the L1-loop in place, resulting in the L1-loop moving outward which in turn allows translation of the MX-helix towards the membrane inner leaflet (Fig. S1).

Conclusion

Our results, investigate the mobility of the cytosolic end of the MA-helices by using a disulfide chemistry approach. Intersubunit cross-linking through agonist-activation/oxidation three helical turns below the lateral portals leads to smaller macroscopic currents and compromises activation gating (de la Pena, Alonso-Ron et al. 2011). This may indicate that mobility/flexibility of the MA-helices below the lateral portals is required to open the cytosolic ion pathway. In contrast, disulfide formation at the cytosolic end of the MA-helices, where the helices converge, is functionally silent. The absence of a functional effect of this disulfide formation further confirms that ions do not exit the cytosolic vestibule along the long channel absence, but instead through five lateral portals that open through concerted conformational changes involving MA-helices and L1-loops. Further studies are needed to experimentally and/or computationally investigate the concerted mechanism.

Author Contributions:

M.J. and A.G.S. designed research. A.G.S. performed experiments. A.G.S and M.J analyzed data. A.G.S. and M.J. wrote the paper.

Acknowledgments:

Research reported in this publication was supported by the National Institute of Neurological Disorders and Stroke of the National Institutes of Health under award number R01NS077114 (to MJ). The content is solely the responsibility of the authors and does not necessarily represent the official views of the National Institutes of Health. We thank the TTUHSC Core Facilities: some of the images and or data were generated in the Image Analysis Core Facility & Molecular Biology Core Facility supported by TTUHSC.

The authors declare no conflict of interest.

Tables

Table 1: Distances (in Å) between engineered cysteines and pore diameters in different X-ray and cryo-EM structures, as measured in Pymol.

	L402C/L403C			L409C/L409C		
PDB	Across the pore	L402C-L403C	L402C-L402C	Across the pore	I409C-I410C	I409C-I409C
4PIR x-ray	13	6.1	7.8	12.9	5.7	8.0

6BE1 (Apo-closed)	14.7	7.3	9.4	13.6	7.4	9.1
6HIS (T inhibited)	14.6	6.9	9.0	14.2	6.3	8.8
6HIQ (I2 intermediate)	14.8	6.9	8.9	13.6	6.0	8.6
6DG8 (State 2 open)	15.4	7.7	9.0	15.3	8.3	9.5

Figures

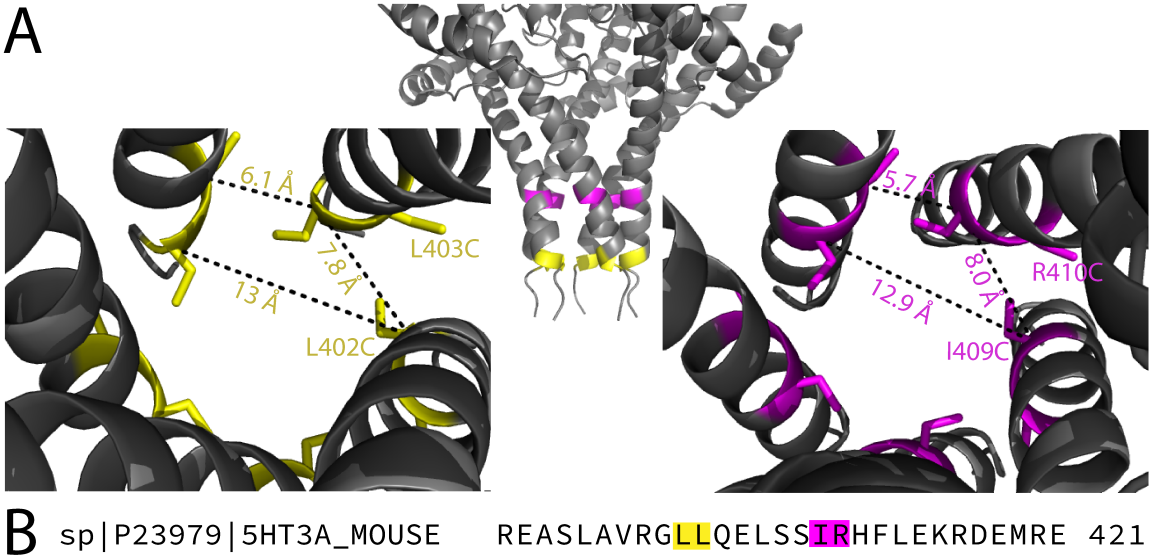

Figure 1. **Structural representation of Cysteine pairs within the MA-helices.** (**A**) (middle panel) Cartoon representation (PDB: 4PIR (Hassaine, Deluz et al. 2014)) of 5-HT_{3A}-ICD viewed parallel to the membrane. Yellow (L402/L403) and magenta (I409/R410) residues represent the Cys pairs. (left and right panel) Cartoon representations of the ICD of 5-HT_{3A}, viewed down the pore, showing L402C/L403C (yellow, left) and I409C/R410C (magenta) residues and the distances between their α-carbons. **(B)** Sequence of part of the m5-HT_{3A} MA α-helix (R393 to E421) with the amino acids mutated to Cys highlighted (yellow: L402/L403, magenta: I409/R410).

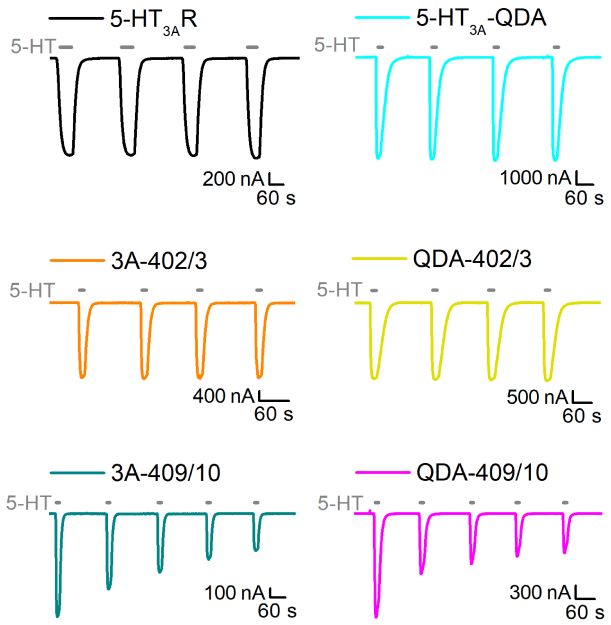

Figure 2. Stability of agonist (5-HT)-induced current amplitudes. Sample traces of currents recorded from *X. laevis* oocytes expressing 5-HT_{3A} wildtype and engineered constructs in response to 3 µM 5-HT (grey bars). 5-HT_{3A}R (black), 5-HT_{3A}-QDA (teal), 3A-402/403 (orange), and QDA-402/403 (yellow) show stable responses to repeated applications of the agonist. Bottom panel: 3A-409/410 and QDA-409/410 show successively decreasing current amplitudes with each 5-HT-application until a stable response is reached.

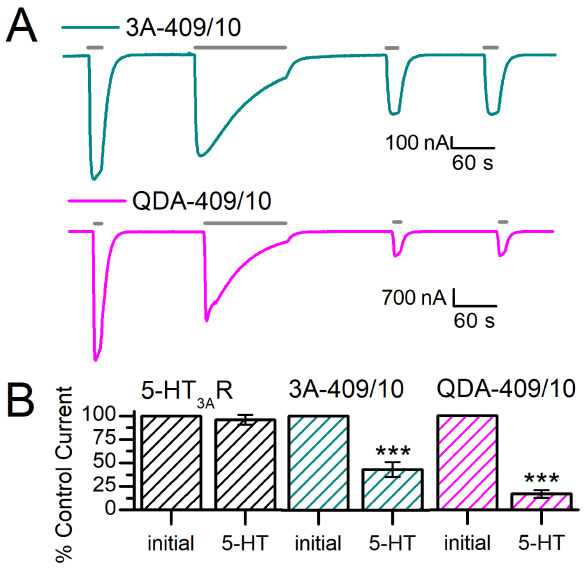

Figure 3. Prolonged agonist (5-HT) exposure in 409/410 Cys pairs leads to stable, decreased current responses. (A) Sample traces of 3A-409/410 (green) and QDA-409/410 (magenta) in response to 3 μM 5-HT (grey bars). The initial inward current represents the reference current amplitude (100% of current) and is followed by an agonist application of 2 min. After this prolonged 5-HT exposure, both Cys pairs exhibit reduced but stable inward currents. **(B)** Quantification of the reduced current amplitudes after prolonged agonist application in 5-HT_{3A} (black), 3A-409/410 (green), and QDA-409/410 (magenta). Data is shown as mean±S.D. (n≥3). Statistical significance was determined with paired t-test between the initial inward current and the stable, reduced current amplitude after the elongated 5-HT exposure (*p≤0.05 **p≤0.01 ***p≤0.001).

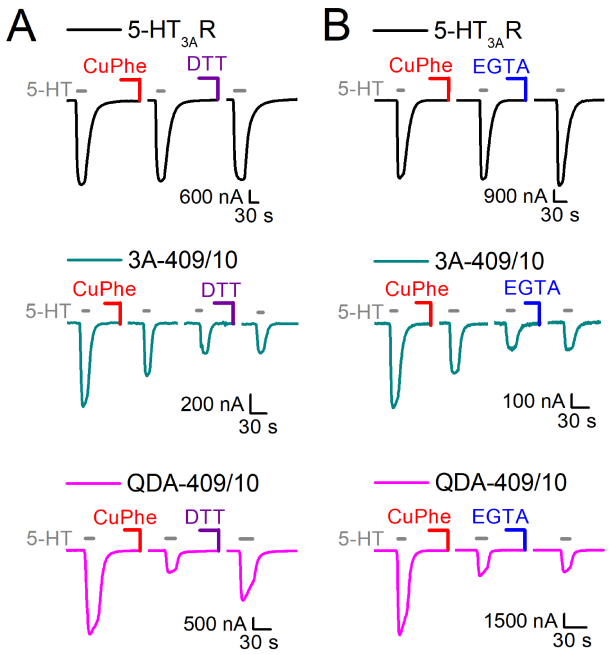

Figure 4. Effect of oxidizing (Cu:Phe), reducing (DTT), and chelating (EGTA) agents on 5-HT$_{3A}$ and 409/410 Cys pairs. (A) Sample traces of 5-HT$_{3A}$R (black), 3A-409/410 (green), and QDA-409/410 (magenta). The inward currents were evoked with 3 μM 5-HT. The initial inward current represents the reference current amplitude (100% of current). Following the 5-HT application(s), the oocytes were exposed to 2 min of Cu:Phe (100:200 μM) and then a 6 min wash with OR-2 (not pictured) before another application of 5-HT (second inward current depicted). 5-HT was applied until a stable current response was achieved (stable response to 5-HT is the inward current before DTT, labeled "self" in Fig 4 for 409/410 mutants). Lastly, 10 mM DTT was applied to the oocytes for 2 min, followed by a 6 min OR-2 wash (not pictured) and 5-HT (last inward current pictured). **(B)** Sample traces of 5-HT$_{3A}$R (black), 3A-409/410 (green), and QDA-409/410 (magenta). Same experimental set-up as in **(A)** but during the last step 1 mM EGTA was applied instead of DTT.

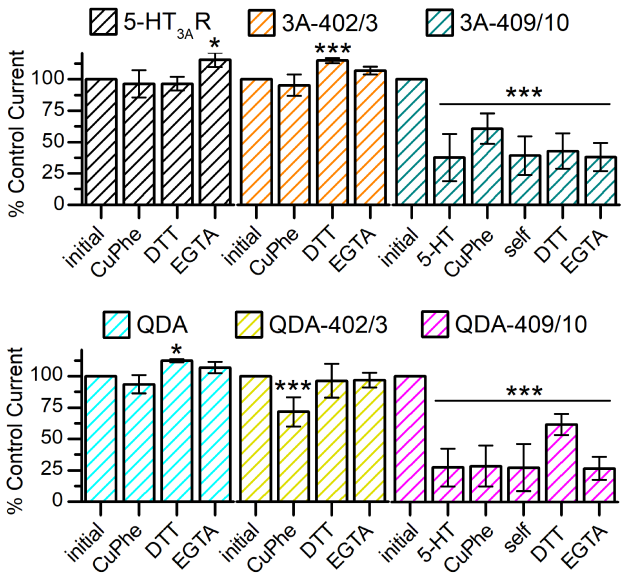

Figure 5. Quantification of agonist (5-HT)-induced current amplitudes in response to agonist, oxidizing (Cu:Phe), reducing (DTT), or chelating agent (EGTA). Quantitative representation of current amplitudes for Fig 2, 4, and S3. The initial inward current represents 100% of the current response. Data is shown as mean±S.D. ($n \geq 3$). Statistical significance was determined with one-way ANOVA, Dunnett's multiple comparisons test between the initial inward current and each set of conditions (*$p \leq 0.05$ **$p \leq 0.01$ ***$p \leq 0.001$).

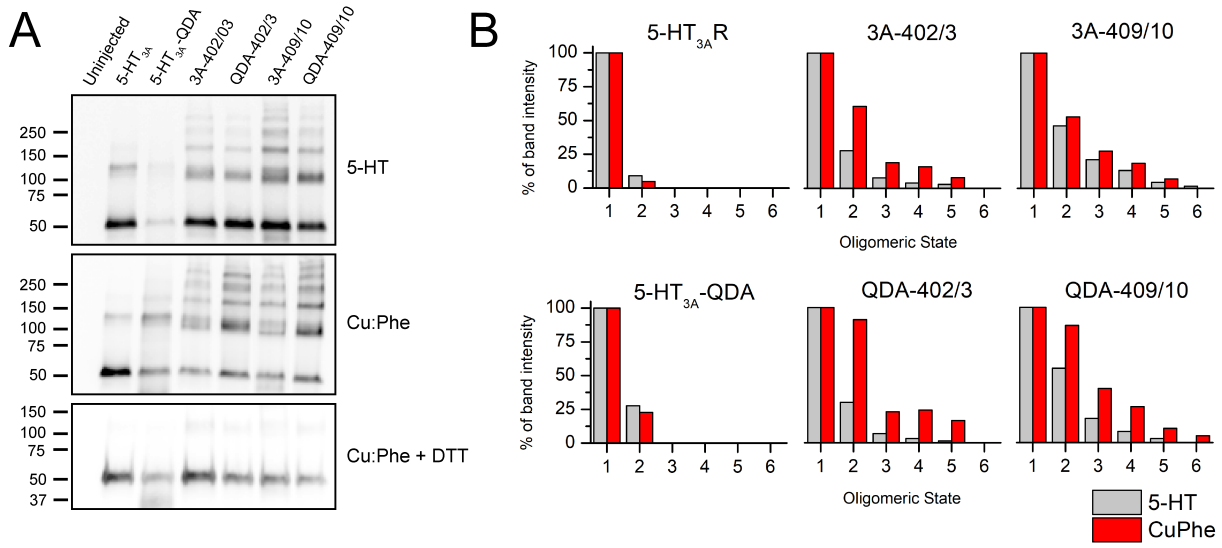

Figure 6. Cross-linking analyzed after SDS-PAGE separation and Western Blot. (A) 5-HT_{3A} and construct-expressing *X. laevis* oocytes were treated to mimic the electrophysiology experiments (either exposed to 2 min of 3 μM 5-HT or 100:200 μM Cu:Phe). Band intensity varied with oocyte expression levels and loading was adjusted accordingly. SDS-PAGE fractions were run with and without reducing agent to show covalent oligomerization of the channels (top panel). Monomers (55 kD) are seen for all constructs, higher cross-linked oligomeric states for all double-Cys mutants. Note, the band running at a slightly higher molecular weight than dimers is seen in all samples (~130 kDa). (Bottom panel) total protein fractions were run with reducing agent (DTT) to show release of the cross-link through disulfide reduction. **(B)** Quantification of band intensity (UN-SCAN-IT *gel*™). Monomer bands were used as control (100%) for each construct with each condition.

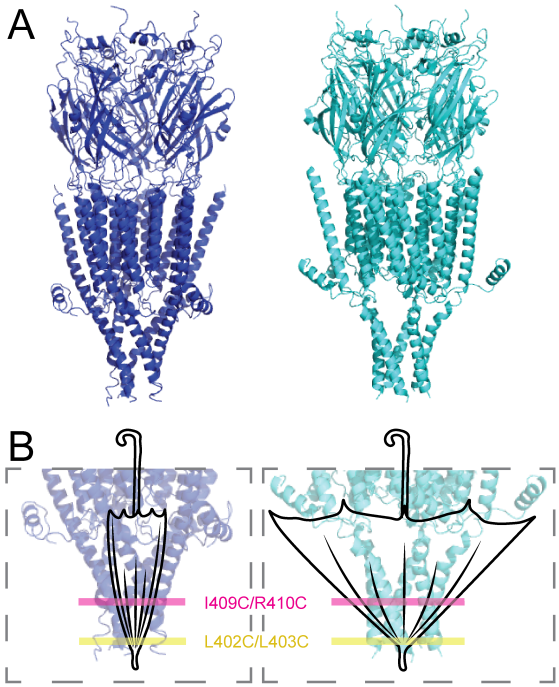

Figure 7. Umbrella analogy of MA-helix mobility. The MA-helices move in a comparable fashion between closed and open states, as do umbrella rods between closed and open states. The L402C/L403C (yellow) is located closer to the top notch, where the rods of the umbrella converge, and I409C/R410C (magenta) is further away from the ferrule. When the umbrella is closed (the receptor is in a non-conducting state – blue (PDB: 6BE1 (Basak, Gicheru et al. 2018))), the rods are aligned with the shaft of the umbrella. The rods are stretched away when the canopy opens (receptor in a conducting state – cyan (PDB: 6DG8 (Basak, Gicheru et al. 2018))). Note that the distance changes between rod positions closer to the ferrule/top notch are miniscule and increase with increasing distance to the ferrule.

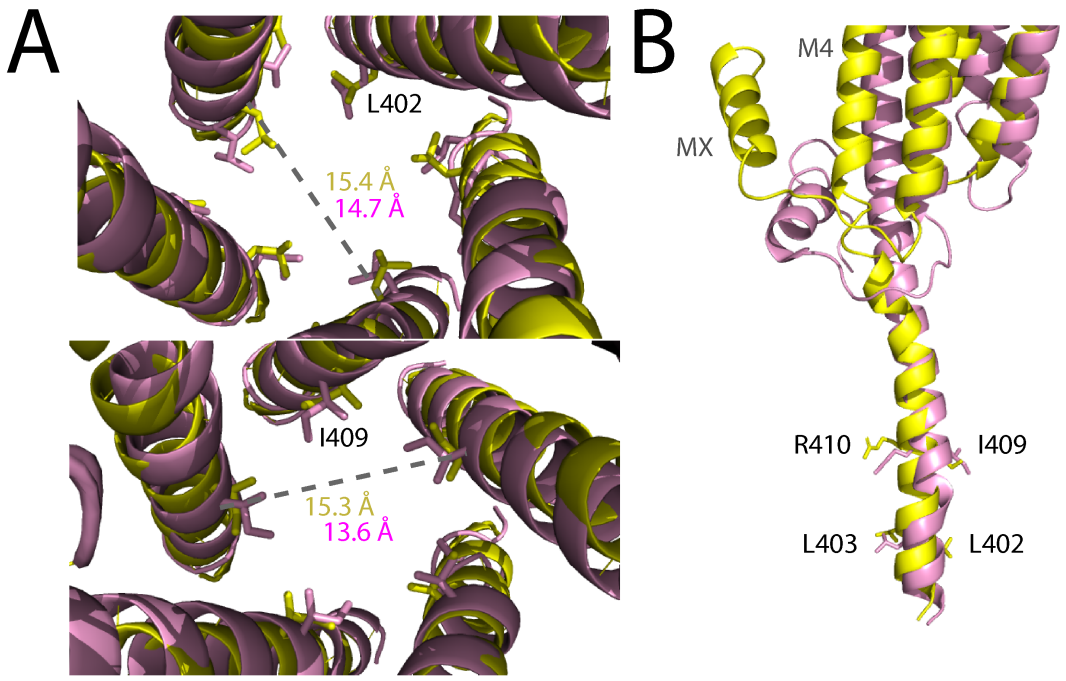

Figure S1. Alignment of 5-HT$_{3A}$ Apo (6BE1, pink (Basak, Gicheru et al. 2018)) and State 2 (6DG8, yellow (Basak, Gicheru et al. 2018)). (A) View down the pore of the ICD of 5-HT$_{3A}$. Side chains visible for L402/L403 (top panel) and I409/R410 (bottom panel) as well as the pore diameter for the different structures. **(B)** Alignment of a single subunit of 5-HT$_{3A}$, cartoon representation, emphasizing the differences between the open and closed conducting states.

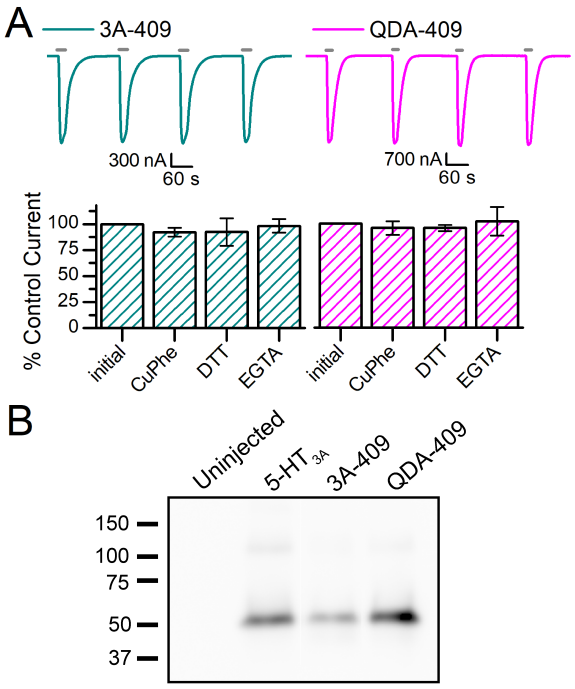

Figure S2. **Evaluation of single Cys at 409 in response to 5-HT, Cu:Phe, DTT, and EGTA. (A)** (top panel) Sample traces of 3A-409 and QDA-409 in response to 3 μM 5-HT, showing stable current amplitudes with each agonist application. (bottom panel) Quantification of current amplitudes after 3A-409 and QDA-409 were exposed to Cu:Phe (100:200 μM), 10 mM DTT, and 1mM EGTA. The first inward current recorded in response to 3 μM 5-HT is the reference current amplitude (100% of current). Experimental set-up was the same as in Fig. 4. Data is shown as mean±S.D. (n≥3). Statistical significance was determined with one-way ANOVA, Dunnett's multiple comparisons test between the initial inward current and each set of conditions. (B) Western blots of single Cys pairs and uninjected oocytes and 5-HT_{3A} as controls. Experimental set-up was the same as in Fig. 6. Expressing *X. laevis* oocytes were exposed to 2 min of 100:200 μM Cu:Phe. SDS-PAGE fractions were run without reducing agent.

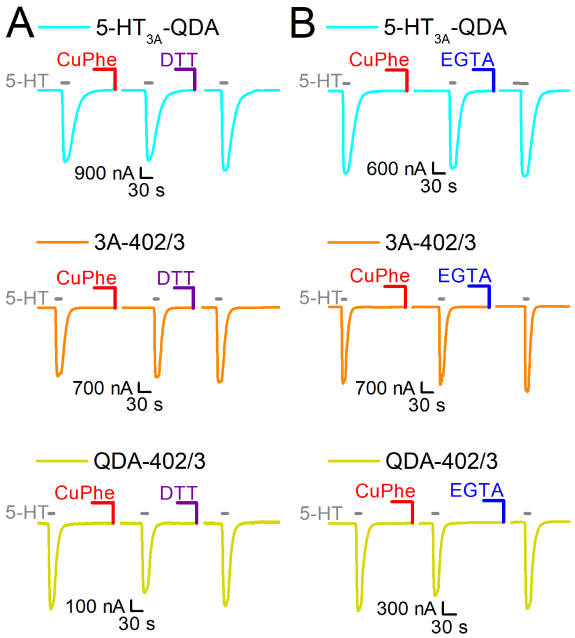

Figure S3. **Effect of Cu:Phe, DTT, and EGTA on QDA and 402/403 Cys pairs. (A)** Sample traces of QDA (cyan), 3A-402/03 (orange), and QDA-402/403 (yellow). The inward currents were evoked with 3 μM 5-HT (grey bars). The initial inward current represents the reference current amplitude (100% of current). Following the 5-HT application(s), the oocytes were exposed to 2 min of Cu:Phe (100:200 μM) and then a 6 min wash with OR-2 (not pictured) before another application of 5-HT (second inward current depicted). 5-HT was applied until a stable current response was achieved (stable response to 5-HT is the inward current before DTT, labeled "self" in Fig 4 for 409/410 mutants). Lastly, 10 mM DTT was applied to the oocytes for 2 min, followed by a 6 min OR-2 wash (not pictured) and 5-HT (last inward current pictured). **(B)** Sample traces of QDA (cyan), 3A-402/403 (orange), and QDA-402/403 (yellow). Same experimental set-up as in **(A)** but during the last step 1 mM EGTA was applied instead of DTT.

References (at the end, convert to numbers)

Amin, D. N., B. L. Taylor and M. S. Johnson (2006). "Topology and boundaries of the aerotaxis receptor Aer in the membrane of Escherichia coli." J Bacteriol **188**(3): 894-901.
Bali, M., M. Jansen and M. H. Akabas (2009). "GABA-induced intersubunit conformational movement in the GABAA receptor alpha 1M1-beta 2M3 transmembrane subunit interface: experimental basis for homology modeling of an intravenous anesthetic binding site." J Neurosci **29**(10): 3083-3092.
Baptista-Hon, D. T., T. Z. Deeb, J. J. Lambert, J. A. Peters and T. G. Hales (2013). "The minimum M3-M4 loop length of neurotransmitter-activated pentameric receptors is critical for the structural integrity of cytoplasmic portals." J Biol Chem **288**(30): 21558-21568.
Basak, S., Y. Gicheru, S. Rao, M. S. P. Sansom and S. Chakrapani (2018). "Cryo-EM reveals two distinct serotonin-bound conformations of full-length 5-HT3A receptor." Nature **563**(7730): 270-274.
Basak, S., Y. Gicheru, A. Samanta, S. K. Molugu, W. Huang, M. Fuente, T. Hughes, D. J. Taylor, M. T. Nieman, V. Moiseenkova-Bell and S. Chakrapani (2018). "Cryo-EM structure of 5-HT3A receptor in its resting conformation." Nat Commun **9**(1): 514.
Bass, R. B., S. L. Butler, S. A. Chervitz, S. L. Gloor and J. J. Falke (2007). "Use of site-directed cysteine and disulfide chemistry to probe protein structure and dynamics: applications to soluble and transmembrane receptors of bacterial chemotaxis." Methods Enzymol **423**: 25-51.
Bera, A. K. and M. H. Akabas (2005). "Spontaneous thermal motion of the GABA(A) receptor M2 channel-lining segments." J Biol Chem **280**(42): 35506-35512.
Borghese, C. M., J. A. Hicks, D. J. Lapid, J. R. Trudell and R. A. Harris (2014). "GABA(A) receptor transmembrane amino acids are critical for alcohol action: disulfide cross-linking and alkyl methanethiosulfonate labeling reveal relative location of binding sites." J Neurochem **128**(3): 363-375.
Careaga, C. L. and J. J. Falke (1992). "Thermal motions of surface alpha-helices in the D-galactose chemosensory receptor. Detection by disulfide trapping." J Mol Biol **226**(4): 1219-1235.
Carland, J. E., M. A. Cooper, M. R. Livesey, T. G. Hales, J. A. Peters and J. J. Lambert (2013). "Mutagenic analysis of the intracellular portals of the human 5-HT3A receptor." J Biol Chem **288**(44): 31592-31601.
Chrisman, P. A., J. I. Podair, E. M. Jobe and M. M. Levandoski (2014). "Intra-subunit flexibility underlies activation and allosteric modulation of neuronal nicotinic acetylcholine receptors." Neuropharmacology **79**: 420-431.
de la Pena, P., C. Alonso-Ron, A. Machin, J. Fernandez-Trillo, L. Carretero, P. Dominguez and F. Barros (2011). "Demonstration of physical proximity between the N terminus and the S4-S5 linker of the human ether-a-go-go-related gene (hERG) potassium channel." J Biol Chem **286**(21): 19065-19075.
Du, J., W. Lu, S. Wu, Y. Cheng and E. Gouaux (2015). "Glycine receptor mechanism elucidated by electron cryo-microscopy." Nature **526**(7572): 224-229.
Fisher, A. E., T. A. Hague, C. L. Clarke and D. P. Naughton (2004). "Catalytic superoxide scavenging by metal complexes of the calcium chelator EGTA and contrast agent EHPG." Biochem Biophys Res Commun **323**(1): 163-167.
Gharpure, A., J. Teng, Y. Zhuang, C. M. Noviello, R. M. Walsh, Jr., R. Cabuco, R. J. Howard, N. T. Zaveri, E. Lindahl and R. E. Hibbs (2019). "Agonist Selectivity and Ion Permeation in the alpha3beta4 Ganglionic Nicotinic Receptor." Neuron.
Goyal, R., A. A. Salahudeen and M. Jansen (2011). "Engineering a prokaryotic Cys-loop receptor with a third functional domain." J Biol Chem **286**(40): 34635-34642.
Halevi, S., J. McKay, M. Palfreyman, L. Yassin, M. Eshel, E. Jorgensen and M. Treinin (2002). "The C. elegans ric-3 gene is required for maturation of nicotinic acetylcholine receptors." EMBO J **21**(5): 1012-1020.
Halevi, S., L. Yassin, M. Eshel, F. Sala, S. Sala, M. Criado and M. Treinin (2003). "Conservation within the RIC-3 gene family. Effectors of mammalian nicotinic acetylcholine receptor expression." J Biol Chem **278**(36): 34411-34417.

Hassaine, G., C. Deluz, L. Grasso, R. Wyss, M. B. Tol, R. Hovius, A. Graff, H. Stahlberg, T. Tomizaki, A. Desmyter, C. Moreau, X. D. Li, F. Poitevin, H. Vogel and H. Nury (2014). "X-ray structure of the mouse serotonin 5-HT3 receptor." Nature **512**(7514): 276-281.
Ilegems, E., H. Pick, C. Deluz, S. Kellenberger and H. Vogel (2005). "Ligand binding transmits conformational changes across the membrane-spanning region to the intracellular side of the 5-HT3 serotonin receptor." Chembiochem **6**(12): 2180-2185.
Jansen, M. and M. H. Akabas (2006). "State-dependent cross-linking of the M2 and M3 segments: functional basis for the alignment of GABAA and acetylcholine receptor M3 segments." J Neurosci **26**(17): 4492-4499.
Jansen, M., M. Bali and M. H. Akabas (2008). "Modular design of Cys-loop ligand-gated ion channels: functional 5-HT3 and GABA rho1 receptors lacking the large cytoplasmic M3M4 loop." J Gen Physiol **131**(2): 137-146.
Kelley, S. P., J. I. Dunlop, E. F. Kirkness, J. J. Lambert and J. A. Peters (2003). "A cytoplasmic region determines single-channel conductance in 5-HT3 receptors." Nature **424**(6946): 321-324.
Kobashi, K. (1968). "Catalytic oxidation of sulfhydryl groups by o-phenanthroline copper complex." Biochim Biophys Acta **158**(2): 239-245.
Kozuska, J. L., I. M. Paulsen, W. J. Belfield, I. L. Martin, D. J. Cole, A. Holt and S. M. Dunn (2014). "Impact of intracellular domain flexibility upon properties of activated human 5-HT3 receptors." Br J Pharmacol **171**(7): 1617-1628.
Lee, C. H. and E. Gouaux (2011). "Amino terminal domains of the NMDA receptor are organized as local heterodimers." PLoS One **6**(4): e19180.
Livesey, M. R., M. A. Cooper, T. Z. Deeb, J. E. Carland, J. Kozuska, T. G. Hales, J. J. Lambert and J. A. Peters (2008). "Structural determinants of Ca2+ permeability and conduction in the human 5-hydroxytryptamine type 3A receptor." J Biol Chem **283**(28): 19301-19313.
Miyazawa, A., Y. Fujiyoshi, M. Stowell and N. Unwin (1999). "Nicotinic acetylcholine receptor at 4.6 A resolution: transverse tunnels in the channel wall." J Mol Biol **288**(4): 765-786.
Mnatsakanyan, N. and M. Jansen (2013). "Experimental determination of the vertical alignment between the second and third transmembrane segments of muscle nicotinic acetylcholine receptors." J Neurochem **125**(6): 843-854.
Mnatsakanyan, N., S. N. Nishtala, A. Pandhare, M. C. Fiori, R. Goyal, J. E. Pauwels, A. F. Navetta, A. Ahrorov and M. Jansen (2015). "Functional Chimeras of GLIC Obtained by Adding the Intracellular Domain of Anion- and Cation-Conducting Cys-Loop Receptors." Biochemistry **54**(16): 2670-2682.
Morales-Perez, C. L., C. M. Noviello and R. E. Hibbs (2016). "X-ray structure of the human alpha4beta2 nicotinic receptor." Nature **538**(7625): 411-415.
Pandhare, A., A. S. Pappu, H. Wilms, M. P. Blanton and M. Jansen (2017). "The antidepressant bupropion is a negative allosteric modulator of serotonin type 3A receptors." Neuropharmacology **113**(Pt A): 89-99.
Pandhare, A., E. Pirayesh, A. G. Stuebler and M. Jansen (2019). "Triple arginines as molecular determinants for pentameric assembly of the intracellular domain of 5-HT3A receptors." J Gen Physiol **151**(9): 1135-1145.
Papke, D. and C. Grosman (2014). "The role of intracellular linkers in gating and desensitization of human pentameric ligand-gated ion channels." J Neurosci **34**(21): 7238-7252.
Pirayesh, E., A. G. Stuebler, A. Pandhare and M. Jansen (2019). "Delineating the Site of Interaction of the 5-HT3A Receptor with the Chaperone Protein RIC-3." Biophys J.
Polovinkin, L., G. Hassaine, J. Perot, E. Neumann, A. A. Jensen, S. N. Lefebvre, P. J. Corringer, J. Neyton, C. Chipot, F. Dehez, G. Schoehn and H. Nury (2018). "Conformational transitions of the serotonin 5-HT3 receptor." Nature **563**(7730): 275-279.

Reeves, D. C., E. N. Goren, M. H. Akabas and S. C. Lummis (2001). "Structural and electrostatic properties of the 5-HT3 receptor pore revealed by substituted cysteine accessibility mutagenesis." J Biol Chem **276**(45): 42035-42042.
Sauguet, L., A. Shahsavar, F. Poitevin, C. Huon, A. Menny, A. Nemecz, A. Haouz, J. P. Changeux, P. J. Corringer and M. Delarue (2014). "Crystal structures of a pentameric ligand-gated ion channel provide a mechanism for activation." Proc Natl Acad Sci U S A **111**(3): 966-971.
Schmidt, B., L. Ho and P. J. Hogg (2006). "Allosteric disulfide bonds." Biochemistry **45**(24): 7429-7433.
Stuebler, A. G. and M. Jansen (2019). "Bupropion inhibits serotonin type 3AB heteromeric channels at clinically relevant concentrations." Mol Pharmacol.
Thompson, A. J. and S. C. Lummis (2007). "The 5-HT3 receptor as a therapeutic target." Expert Opin Ther Targets **11**(4): 527-540.
Thompson, A. J. and S. C. Lummis (2013). "Discriminating between 5-HT(3)A and 5-HT(3)AB receptors." Br J Pharmacol **169**(4): 736-747.
Unwin, N. (2005). "Refined structure of the nicotinic acetylcholine receptor at 4A resolution." J Mol Biol **346**(4): 967-989.
van Montfort, B. A., G. K. Schuurman-Wolters, R. H. Duurkens, R. Mensen, B. Poolman and G. T. Robillard (2001). "Cysteine cross-linking defines part of the dimer and B/C domain interface of the Escherichia coli mannitol permease." J Biol Chem **276**(16): 12756-12763.
Walsh, R. M., Jr., S. H. Roh, A. Gharpure, C. L. Morales-Perez, J. Teng and R. E. Hibbs (2018). "Structural principles of distinct assemblies of the human alpha4beta2 nicotinic receptor." Nature **557**(7704): 261-265.
Wiltfong, R. E. and M. Jansen (2009). "Probing protein packing surrounding the residues in and flanking the nicotinic acetylcholine receptor M2M3 loop." J Neurosci **29**(6): 1626-1635.